Special Issue

Photoreceptor-Based Biomarkers in AOSLO Retinal Imaging

Katie M. Litts,[1] Robert F. Cooper,[2,3] Jacque L. Duncan,[4] and Joseph Carroll[1,5]

[1]Department of Ophthalmology & Visual Sciences, Medical College of Wisconsin, Milwaukee, Wisconsin, United States
[2]Department of Psychology, University of Pennsylvania, Philadelphia, Pennsylvania, United States
[3]Department of Ophthalmology, University of Pennsylvania, Philadelphia, Pennsylvania, United States
[4]Department of Ophthalmology, University of California, San Francisco, California, United States
[5]Department of Cell Biology, Neurobiology and Anatomy, Medical College of Wisconsin, Milwaukee, Wisconsin, United States

Correspondence: Joseph Carroll, Department of Ophthalmology & Visual Sciences, Medical College of Wisconsin, 925 N 87th Street, Milwaukee, WI 53226-0509, USA; jcarroll@mcw.edu.

Submitted: March 14, 2017
Accepted: July 28, 2017

Citation: Litts KM, Cooper RF, Duncan JL, Carroll J. Photoreceptor-based biomarkers in AOSLO retinal imaging. *Invest Ophthalmol Vis Sci*. 2017;58:BIO255–BIO267. DOI: 10.1167/iovs.17-21868

Improved understanding of the mechanisms underlying inherited retinal degenerations has created the possibility of developing much needed treatments for these relentless, blinding diseases. However, standard clinical indicators of retinal health (such as visual acuity and visual field sensitivity) are insensitive measures of photoreceptor survival. In many retinal degenerations, significant photoreceptor loss must occur before measurable differences in visual function are observed. Thus, there is a recognized need for more sensitive outcome measures to assess therapeutic efficacy as numerous clinical trials are getting underway. Adaptive optics (AO) retinal imaging techniques correct for the monochromatic aberrations of the eye and can be used to provide nearly diffraction-limited images of the retina. Many groups routinely are using AO imaging tools to obtain in vivo images of the rod and cone photoreceptor mosaic, and it now is possible to monitor photoreceptor structure over time with single cell resolution. Highlighting recent work using AO scanning light ophthalmoscopy (AOSLO) across a range of patient populations, we review the development of photoreceptor-based metrics (e.g., density/geometry, reflectivity, and size) as candidate biomarkers. Going forward, there is a need for further development of automated tools and normative databases, with the latter facilitating the comparison of data sets across research groups and devices. Ongoing and future clinical trials for inherited retinal diseases will benefit from the improved resolution and sensitivity that multimodal AO retinal imaging affords to evaluate safety and efficacy of emerging therapies.

Keywords: adaptive optics, retinal degeneration, retinal imaging, photoreceptor, biomarkers

The rapid development of therapeutic interventions for ophthalmic diseases is providing potential treatments for inherited retinal degenerations. Important for the success of emerging clinical trials will be the ability to evaluate the safety and efficacy of the prospective treatment(s) with high sensitivity. Measures of visual function are accepted commonly as primary endpoints for clinical trials by regulatory agencies because they describe the impact of disease and treatment on the patient's perception of the world.[1] However, as photoreceptor loss occurs slowly in many retinal degenerations, it can take many years to measure changes in visual function reliably using clinically available technologies.[2–4] In clinical trials, waiting years for a measurable change may not be feasible due to time and economic constraints. This necessitates the need for more sensitive, reliable outcome measures to assess treatment safety and efficacy.

It is possible to monitor diseases affecting the retina and the effect of potential therapeutic interventions through direct visualization of individual photoreceptors with tools for high-resolution in vivo imaging of the retina. Adaptive optics (AO), in combination with various other retinal imaging modalities, has revolutionized the way in which we visualize the living human retina.[5,6] AO corrects the monochromatic aberrations of the eye,[7] and when combined with techniques like fundus imaging, scanning laser ophthalmoscopy (SLO), and optical coherence tomography (OCT), the result is nearly diffraction-limited imaging of the living retina.[6,8,9] Compared to currently available clinical tools, this improved resolution makes AO retinal imaging a sensitive method for monitoring retinal degeneration. For example, recent studies using AO retinal imaging in eyes with retinal diseases have demonstrated that significant decreases in cone photoreceptor spatial density and increases in cone spacing are observable before visual acuity becomes abnormal.[10–13] In addition, multiple examples demonstrate a lack of correlation between photoreceptor structure seen with AOSLO and clinical OCT.[14–17] Confocal and non-confocal split-detector AOSLO each have their own advantages and limitations. Despite the exquisite resolution provided by AO-based retinal imaging tools, photoreceptor-based metrics have not been validated as outcome measures for multicenter clinical trials, partly due to the lack of standardized AO-equipped retinal imaging systems and analytical software. Nevertheless, many groups have used AO imaging tools to provide important insight into how retinal degenerations affect photoreceptor survival during disease progression and in response to therapies.[11–13,18–21]

The ultimate use of any ophthalmic imaging modality generally is limited by the ability to extract quantitative information from the images. In this manuscript, we review photoreceptor-based biomarkers (e.g., density/geometry, re-

flectivity, and size) that are being used or have been proposed for analyzing any AO retinal images of the photoreceptor mosaic, with a focus on AOSLO. Through validation and the assessment of reliability and repeatability, these biomarkers may become valuable outcome measures in current and future clinical trials targeting patients with inherited retinal degenerations. In addition, such biomarkers could be useful to assess disease progression and treatment response in animal models of retinal disease, as it now is possible to resolve the cone mosaic in a number of animal models using a variety of imaging tools.[22–28] Beyond measuring treatment response, it is possible that AO retinal imaging could be used to select specific patients for a given treatment, as accurate assessment of remnant cone structure in diseases for which cone-directed gene therapy is being considered would be a requisite step to establish the visual and therapeutic potential of a given retina.[29] An example of this is shown in Figure 1, where two patients with achromatopsia have dramatically different numbers of remnant cones;[17] thus, one might not expect the same therapeutic response in these individuals. Finally, although this review will focus on AOSLO-based photoreceptor biomarkers, it should be noted that AO retinal imaging has many applications in humans, including visualizing RPE,[30–32] blood vessels,[33,34] and ganglion cells (Liu Z, et al. *IOVS* 2017;58:ARVO E-Abstract 3430),[35] that are explored in depth in other reviews.[6,36,37]

Origins of Photoreceptor Signals by AO Retinal Imaging

Before exploring potential biomarkers, it is worth briefly examining the way in which photoreceptors are visualized in AO retinal images. Although there is controversy on the cellular origin of OCT photoreceptor signals from AO-equipped and non-AO OCT,[38–40] there appears to be more consensus about the origin of the signals when using other AO-equipped technology. AO retinal imaging allows for noninvasive imaging of individual cone photoreceptors through increased lateral resolution and photoreceptor waveguiding via the optical Stiles-Crawford effect.[7,41] The visualization of photoreceptors is enabled in part by the high refractive index of the photoreceptor relative to the surrounding interphotoreceptor matrix. The backscattered light at the interface between the outer segments and RPE is coupled back through the cone and provides the directional component of the reflected light.[42–47] Thus, it is thought that for a photoreceptor to be visible by waveguiding, its outer segment must be intact and contacting the RPE apical processes. In OCT, this is seen as an intact interdigization zone (IZ) or cone outer segment tip (COST) band, depending on the technology and imaging system used.[39,48,49] The number of modes a photoreceptor can support depends on the wavelength of light and the diameter of the photoreceptor itself.[44] Thus, while foveal cones only exhibit a single mode (having a Gaussian-like reflectance profile), the larger perifoveal cones may have multiple modes.[42,44] There continues to be extensive work into trying to understand how light interacts with photoreceptors and the source of photoreceptor signals in AO retinal imaging.[46,47]

Conventionally, AOSLO imaging uses a confocal pinhole to detect waveguided light from photoreceptors. AOSLO systems can resolve the smallest cones in the fovea as well as rods in the perifovea and periphery (Fig. 2). Despite excellent resolution, a number of factors interfere with reliable cone visualization. Cones with low reflectivity and with multiple modes or abnormal reflectivity that can occur in some diseases may be missed, counted multiple times, or misidentified as rods. Reflectivity from the RPE also can confound the photoreceptor signal, making the cone mosaic difficult to interpret, especially in eyes with photoreceptor degeneration.[12,50] To guide the analysis of confocal AO retinal imaging, nonconfocal methods can be used. Nonconfocal methods include split-detector AOSLO[51] and the use of one or more offset apertures to collect scattered light from photoreceptors.[35,52] With split-detector AOSLO, the multiple-scattered light is captured by two separate detectors, and signals from

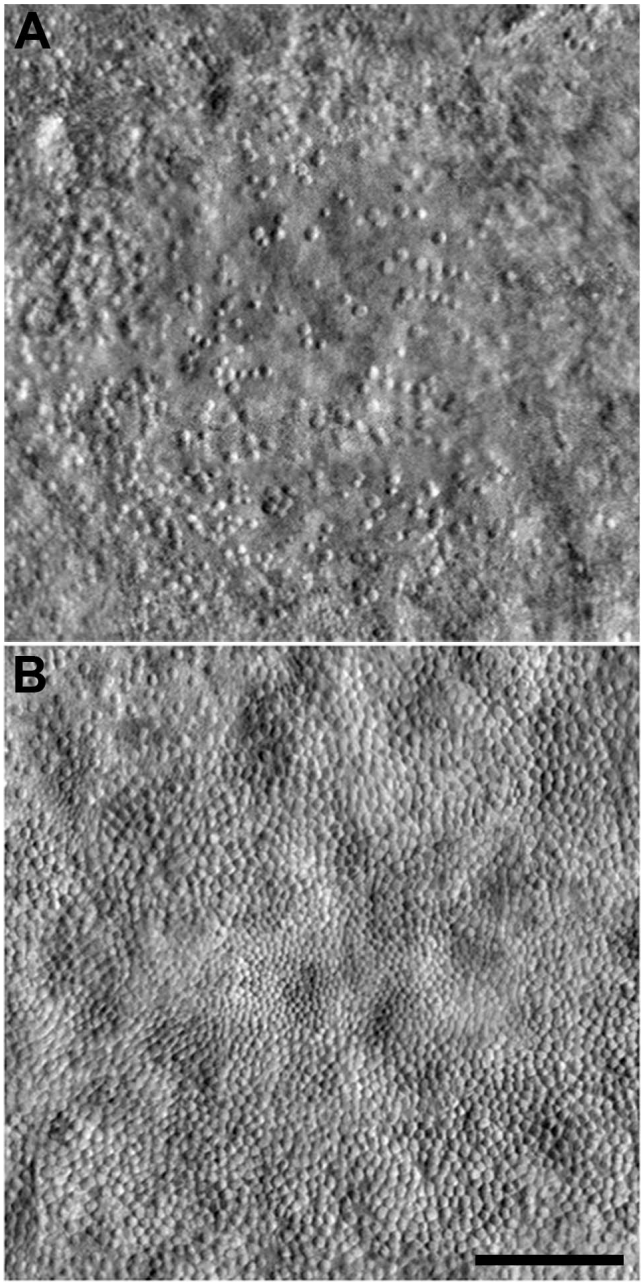

Figure 1. Variability of the foveal cone mosaic in achromatopsia. Split-detector AOSLO images from the right eye of two different subjects with *CNGB3*-associated achromatopsia (and no cone function). (**A**) 16-year-old female with low peak cone density (9917 cones/mm^2). (**B**) 37-year-old male with relatively high peak cone density (44,959 cones/mm^2). Peak cone density was measured as reported by Langlo et al.[17] Implications of this level of interindividual variability in remnant cone structure for defining the therapeutic potential of a given retina remain to be elucidated, though it is worth noting that the visual acuity of these two subjects was markedly different (20/800 for the subject in [**A**] and 20/100 for the subject in [**B**]). *Scale bar*: 100 μm.

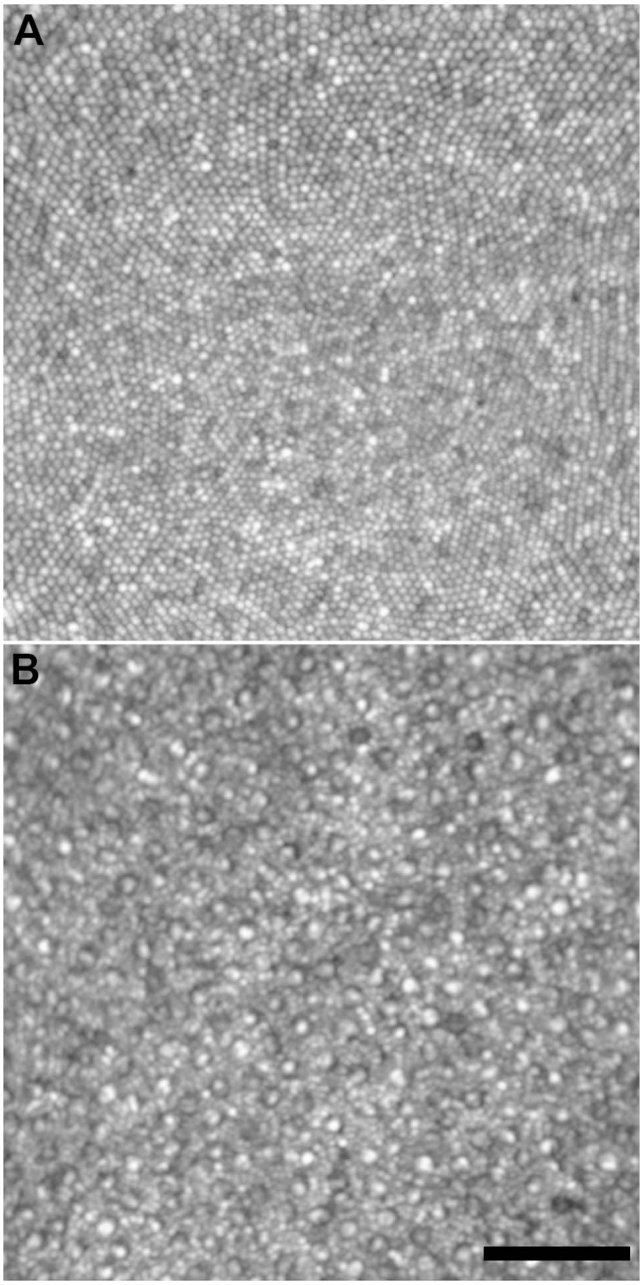

FIGURE 2. Confocal AOSLO images from a normal retina, displayed on a logarithmic scale. (**A**) Tightly packed cones in the fovea and (**B**) Cone and rod mosaic at 10° temporal to fixation. Right eye from a 27-year-old female (JC_11142). *Scale bar*: 50 μm.

both detectors can be subtracted and divided by their sum.[51] This signal is thought to originate from the photoreceptor inner segment, as a recent study showed that the size of the "mound-like" features matched the diameter of cone inner segments from ex vivo histology.[51] Split-detector AOSLO allows for cone inner segments to be imaged in a manner thought to be independent of outer segment integrity (Fig. 3).[16,51] As such, split-detector imaging may be useful for studies of retinal degenerations where the outer segment is affected before the remainder of the photoreceptor, such as achromatopsia,[17,51] retinitis pigmentosa (RP),[53,54] choroideremia,[55,56] and age-related macular degeneration.[57,58] In addition, split-detector imaging could be used to disambiguate reflectivity in confocal imagery arising from cone and noncone structures. As confocal and split-detector AOSLO images can be acquired simultaneously, they should be viewed as complementary imaging modalities for assessing cone structure, each with their own advantages and limitations.

Next, we will explore the use of three general classes of photoreceptor-based biomarkers including photoreceptor density/geometry, reflectivity, and size.

Photoreceptor Density and Geometry

The retinal image itself can be used to extract information about the photoreceptor mosaic. For example, the local orientation of the cone mosaic can be extracted directly from the cone image. Cones in the photoreceptor mosaic are arranged in a regular, but imperfect, triangular lattice.[59] Each cone forms a polygonal "submosaic" with its neighbors, where the locations of a given cone's neighbors form the vertices of the polygon. To quantify the anisotropy of the mosaic, one can extract the "orientation" of each submosaic, defined by the rotation of this polygon.[60–62] This can be done on the scale of an individual submosaic,[60,62] or as an average of submosaics.[61,62] In addition, the modal spacing of the cones (also referred to as intercell distance [ICD]) can be extracted directly from the Fourier transform of the image, which for normal retinas will have an annular appearance – this annulus often is called "Yellott's ring".[61,63–65] There are limitations to this method in that the power spectrum contains information about the object profile itself in addition to the spacing of the objects in the image; this is less of an issue in a contiguously packed mosaic of cells of uniform size, but becomes disabling when working with images of the peripheral photoreceptor mosaic.[65] In addition, the contrast of Yellott's ring often decreases in areas of retinal degeneration or cone loss,[65] making it difficult to extract an accurate estimate of modal spacing. Finally, extracting either average anisotropy or modal spacing relies on the assumption that the mosaic is packed in a regular triangular lattice,[64,66] which often does not hold in eyes with retinal degeneration.

As a result of inherent limitations of these image-based metrics, an important first step in extracting quantitative information about the photoreceptor mosaic often involves the derivation of coordinate locations for the individual cells of interest. Although cones can be identified manually, there are a growing number of effective semiautomated and automated tools.[67–73] Once the cells of interest have been identified in the image, any number of metrics can be calculated automatically. While cell density[15,71,74–81] and ICD[11,18,50,71,80,82–86] are the most commonly used metrics to describe the cone mosaic, there has been a recent expansion to consider other types of metrics, such as percentage of six-sided Voronoi cells, nearest neighbor distance (NND), farthest neighbor distance (FND), nearest neighbor regularity (NNR), linear dispersion index (LDi), number of neighbors regularity (NoNR), Voronoi cell area regularity (VCAR), heterogeneity packing index (HPi), and cell orientation or directionality (Fig. 4).[60,87,88] Together, these metrics have been applied to a wide range of retinal diseases.[12,13,17,18,81,82,88–100] However, it is important to keep in mind that for these metrics, errors in the process of identifying the cones in an image often constrain the repeatability and reliability of a given metric. Thus, it is critical that one understands the capabilities of the particular cone detection algorithm used for their images.[72]

Different metrics have been shown to have markedly different sensitivities for detecting cone loss.[87] While it may seem counterintuitive, the most sensitive metric cannot be assumed to be the best metric across all applications.[87] In other words, for a particular study, the most appropriate metric for analysis should be sensitive enough to detect anticipated

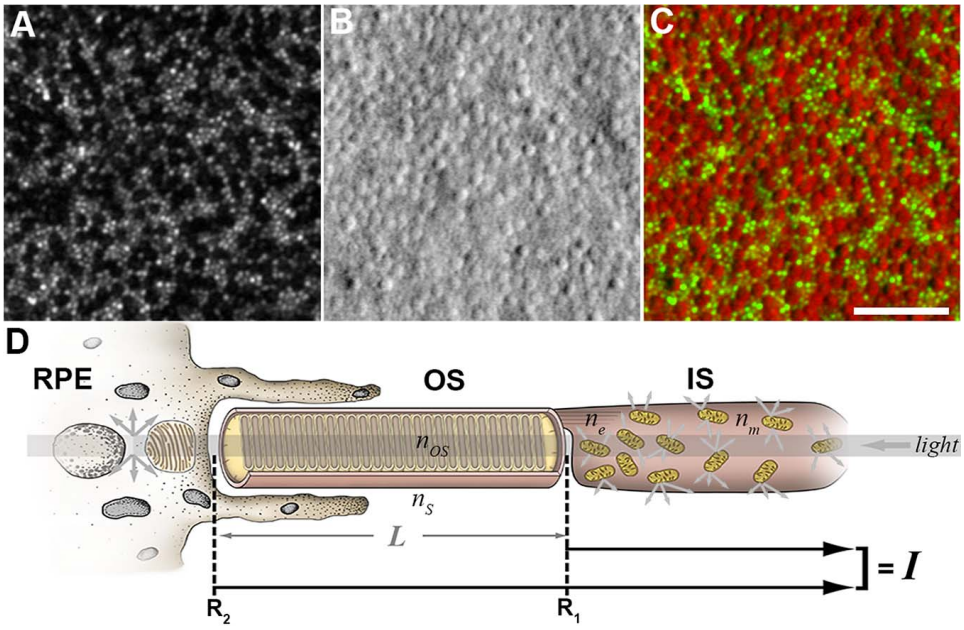

Figure 3. Resolving cone inner and outer segment structure with AOSLO. Shown are confocal (**A**) and split-detection (**B**) images from the parafoveal retina of a patient with *CNGA3*-associated ACHM. The color-merged image (**C**) has the confocal image displayed in *green* and the split-detection image in *red. Scale bar*: 50 μm. (**D**) Photoreceptor schematic based off of a model presented by Jonnal et al.[149] – the signal (*I*) requires intact photoreceptors[42,149] and can vary as a result of small perturbations in photoreceptor structure. Multiply-scattered light from the RPE and inner segments is rejected by confocal AOSLO.

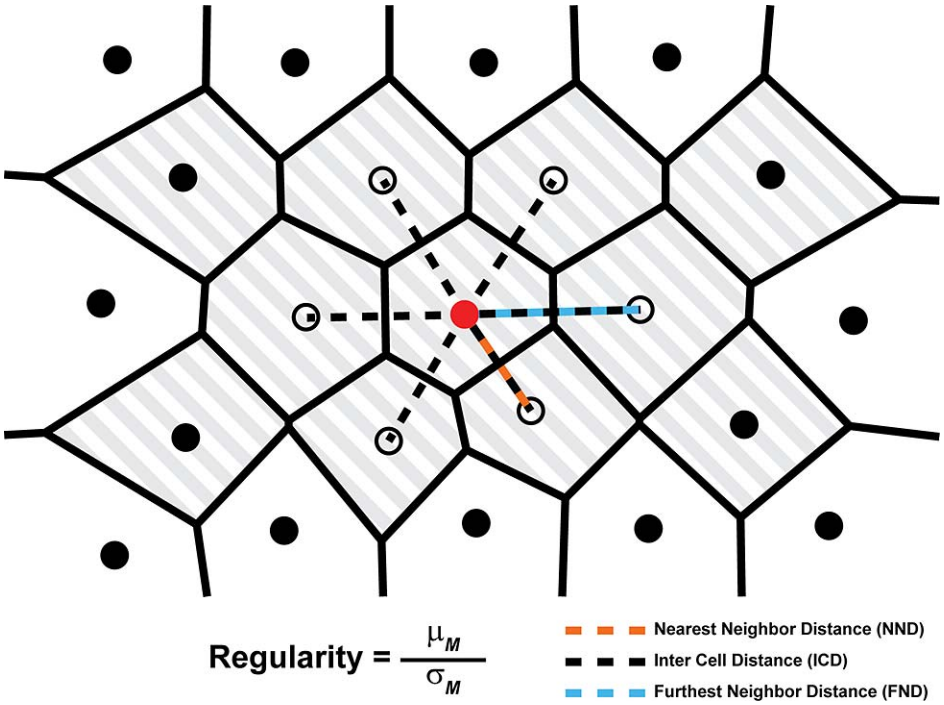

Figure 4. A schematic of a hexagonally arranged patch of cones illustrating the relationship between the distance measurements used by Cooper et al.[87] A single cone (*red circle*) and its six closest neighbors (*open circles*) are highlighted for clarity. The NND is defined as the distance from a given cone to its closest neighbor (*orange dashed line*). The FND is defined as the distance from each cone to its most distant neighbor (*blue dashed line*), and ICD is defined as the average distance between a cone and all of its neighbors (*dashed lines*). To mitigate boundary effects, only cones with bound Voronoi regions (*shaded region*) are included when calculating each metric. The regularity of each of these metrics (M) is defined as the mean (μ_M) of the metric for all cones with bounded Voronoi cells, divided by the metric's SD (σ_M). Reprinted from Cooper RF, Wilk MA, Tarima S, Carroll J. Evaluating descriptive metrics of the human cone mosaic. *Invest Ophthalmol Vis Sci*. 2016;57:2992–3001. Licensed under a Creative Commons Attribution-NonCommercial-NoDerivatives 4.0 International License.

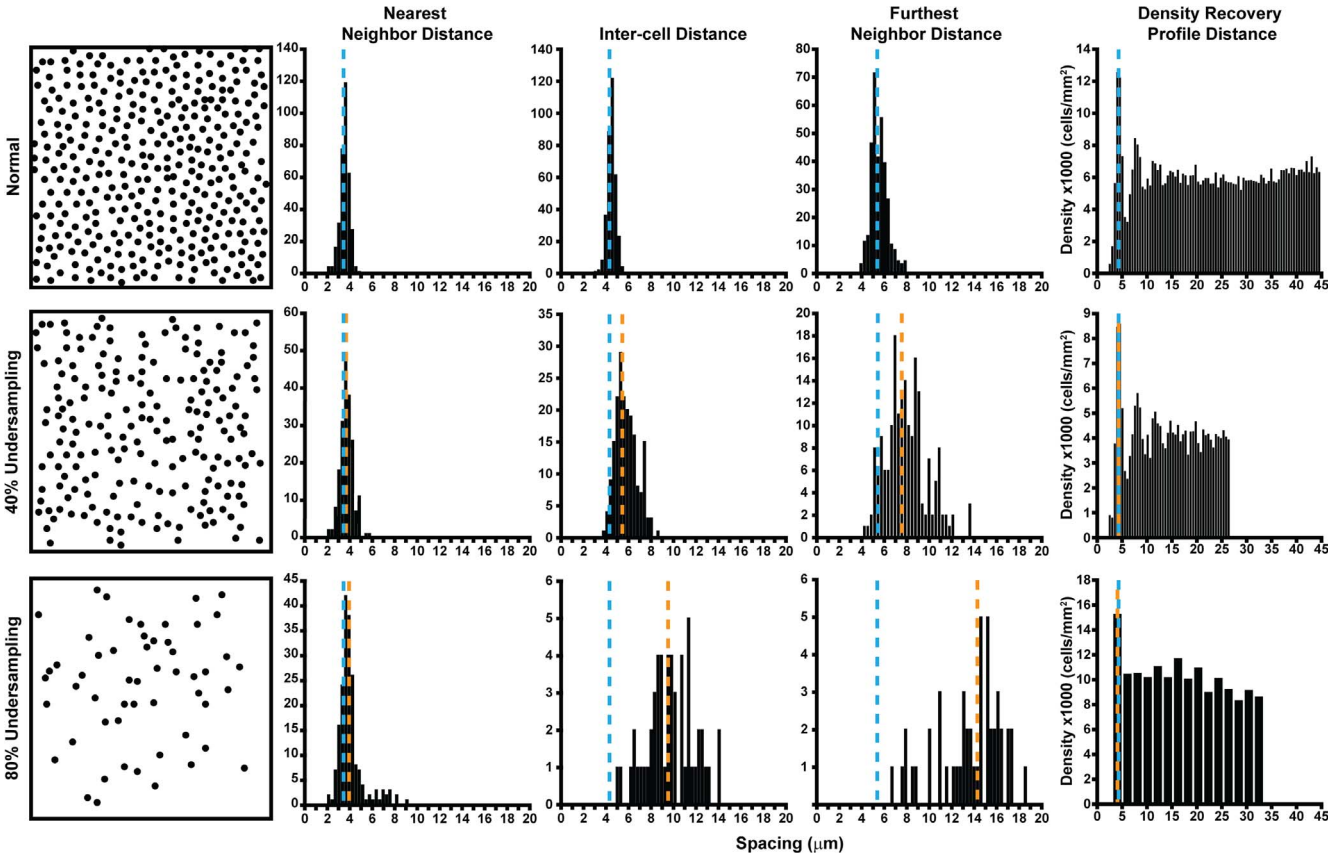

FIGURE 5. Sensitivity and robustness of metrics in detecting cone loss. An illustration of the effect of cone undersampling on histograms of cell distances (NND, ICD, FND) and the DRPD from a single subject (JC_10145). A region of interest (37 × 37 μm sampling window) at 200 μm from the fovea was selected from confocal AOSLO, and cone coordinates were seminautomatically identified. For undersampled mosaics, 40% and 80% of the cone coordinates from the normal mosaic were removed by random distribution using the randperm MATLAB function of cone coordinate list. These mosaics are illustrated in the first column. In each plot, the *blue dashed line* is the mean of the histogram from the complete mosaic, while the *orange dashed line* is the mean of the histograms from the 40% (*middle row*) and the 80% undersampled mosaics (*bottom row*). On all plots, the *y*-axis is the number of cells within each histogram bin. The NND histogram is only marginally affected (indicated by the similarity in the *blue* and *orange dashed lines*), even with an 80% loss. Similarly, the DRPD is largely unaffected by cell loss; its estimated spacing is only affected when the bin size increases (*bottom right*) due to a decrease in density. In contrast, the mean (indicated by further separation of the *blue* and *orange dashed lines*) and spread of both ICD and FND increase substantially with cell loss. Reprinted from Cooper RF, Wilk MA, Tarima S, Carroll J. Evaluating descriptive metrics of the human cone mosaic. *Invest Ophthalmol Vis Sci*. 2016;57:2992–3001. Licensed under a Creative Commons Attribution-NonCommercial-NoDerivatives 4.0 International License.

abnormalities, but robust enough not to be skewed by errors in cell identification. For example, it recently was shown that NND and density recovery profile distance (DRPD), a method to measure ICD, are relatively insensitive to undersampling; even after half of the cones were removed, the mosaic still was detected as normal (Fig. 5).[87] Thus, spacing metrics like these, which are insensitive to small changes in the mosaic, would provide a conservative measure of photoreceptor survival and be insensitive to early cone loss when monitoring a mosaic over time.[62,87] However, if there is uncertainty in the method used to identify the cone coordinates in the image, such metrics would be attractive as they are robust enough to not be impacted by this noise. Conversely, regularity metrics generally are more sensitive. For example, it was shown that NoNR reliably classifies a mosaic as significantly different from normal when only 10% of cones were removed.[87] At the same time, NoNR and other regularity metrics would be more susceptible to errors in the initial identification of cone coordinates. Disambiguation of real cone degeneration from differences in cone identification is especially important in patients with retinal disease, as visibility of the cone mosaic can be altered or obstructed by inner retinal cysts and microcysts present in conditions, such as cystoid macular edema, RP, macular telangiectasia, and age-related macular degeneration.[82,101–104] Moreover, combining metrics with varying sensitivities may provide a more complete picture of the cone mosaic.[87,88,105] For example, a recent study demonstrated that complementary use of two regularity metrics (LDi and HPi) provided 100% accuracy to discriminate controls from patients with diabetes and no clinical signs of diabetic retinopathy.[88] Finally, it is important to note that most metrics have been applied nearly exclusively to the cone mosaic. As many AO imaging systems also can resolve rod photoreceptors,[9,106–108] it will be important to reexamine these metrics for the rod mosaic. As the cells within the rod and cone submosaics differ in size and density, it will be important to examine how metrics describing these interleaved mosaics "interact" with one another in the normal and diseased retina. However, it seems certain that the behavior of various metrics will vary as a function of retinal eccentricity, as a result of the changing rod-to-cone ratio.

Establishing the reliability and repeatability of each metric is essential to the correct interpretation of data from clinical trials (and to eventual acceptance of a metric by the Food and Drug Administration [FDA]). Importantly, this should be done at multiple centers; thus, inclusion of AO retinal imaging in natural history studies of disease progression offers opportu-

nities to validate different photoreceptor-based metrics.[17,19] Repeatability of cone spacing and density measures has been demonstrated in normal eyes[71,109] and eyes with retinal disease.[62,110–112] Interobserver and interinstrument reliability has been demonstrated for cone density measurements on confocal AOSLO images with good quality,[68,113] but may not apply to poor quality images. However, repeatability is expected to differ between imaging systems based on image quality, individual grader,[112,114] and performance of cone identification algorithm; therefore, individual groups should characterize reliability and repeatability for the system and graders in a given study, addressing intersession repeatability and interobserver reliability, before exploring these metrics in a patient population or for clinical trials.[71,110]

Intraframe distortions due to involuntary eye motion affects the repeatability and accuracy of the resultant mosaic metrics when using scanning systems, such as AOSLO or AO-OCT.[115] This should be taken into account for clinical trials enrolling patients with nystagmus, such as those with achromatopsia, where such distortion is often unavoidable.[19,114] Due to eye motion and a relatively low signal-to-noise ratio, SLO-based image sequences must be registered to minimally-distorted reference frames and averaged to increase the signal-to-noise ratio.[116–119] Recently, an automated reference frame selection algorithm (ARFS) was created to select automatically the best minimally-distorted reference frame from a sequence of confocal AOSLO images by comparing the images across the sequence; the ARFS algorithm performed superiorly to humans and minimized time needed for image processing.[119] However, rapid eye movement and nystagmus remain problematic. Real time eye tracking systems[120,121] and higher image acquisition speed[122,123] may minimize the impact of eye movement on image quality. As flood-illuminated AO systems are largely immune to these motion artifact issues, their images serve as a useful "gold-standard" against which to compare images from scanning systems when validating new mosaic metrics.[115,119]

Another factor affecting many of the above metrics is the size of the sampling window or region of interest over which measurements are made. The method used to select regions of interest, such as at fixed intervals along meridians, manual selection of images with best quality near eccentricity of interest, and along concentric rings, can cause cone density measurements to vary by location and between imaging sessions.[124] The size and orientation of the sampling window also has been shown to impact measurements of cone density.[125,126] This effect is likely to be larger for measurements made near the fovea (where cone density is changing rapidly as a function of eccentricity), compared to peripheral retina where cone density is more uniform.[127] Moreover, any sampling window is subject to "boundary effects," where the photoreceptors on the edge of the window may not fit completely within the window. These cells do not contribute all of their area to a density measurement, nor all of their neighbors for a spacing or regularity measurement, resulting in artefactual values. Excluding cells near the edge is essential for accurate metric results, and can be done using a Voronoi tessellation of the cell locations.[87] Cells that are contained completely within the window will have a Voronoi region that is closed, while those that are not will have an open Voronoi region and should be excluded from analysis. This boundary effect will increase as the size of the sampling window decreases, further underscoring the importance of defining the properties of the sampling window used for measurements. Unfortunately, the lack of a uniform/accepted sampling method across studies and research groups currently limits the ability to compare results across studies, and also obstructs robust applications to clinical trials.

Photoreceptor Reflectivity

One of the most salient features of the photoreceptor mosaic is the cell-to-cell and temporal variability in reflectivity,[43] which is even seen in non-AO images of the cone mosaic.[116,128] Cone reflectivity changes have been observed qualitatively and quantitatively in normal and diseased eyes using confocal AOSLO and flood-illuminated AO.[43,58,82,93,102,129–137] Normal waveguiding cones appear as bright spots, whereas non-waveguiding cones appear dark, suggesting an altered outer segment. Interestingly, a lack of sensitivity or cone function has been observed over areas with reduced or no reflectivity, for example, in color vision deficiencies,[135] achromatopsia,[132–134] Stargardt disease,[93,131] RP,[82] and age-related macular degeneration,[58,138] yet residual sensitivity has been observed in areas with reduced or no reflectivity in macular telangiectasia,[102] age-related macular degeneration,[139] foveolitis,[140] and normal eyes.[130] The relationship between reflectivity in confocal AO retinal imaging and cone function remains to be defined more clearly.

In normal eyes, cones exhibiting low reflectance compared to neighboring cones do not necessarily correlate with decreased sensitivity.[43,130] Cone reflectivity can vary depending on the direction of illumination,[41] and has been observed to change over time (seconds and minutes to hours) and from cone to cone.[43] Long-term variation in cone reflectivity has been suggested to result from outer segment renewal,[141,142] and short-term reflectivity changes have been attributed to phototransduction.[143] Similar to cones, the reflectivity of individual rod photoreceptors has been observed to vary over time in health and disease.[129,144] Additionally, cone reflectivity changes after bleaching of the photopigment, which has been used to identify the spectral identity of individual cones.[145,146] Cone and rod reflectivity could be used as metrics, for example, to distinguish *GNAT2*-associated achromatopsia with higher cone reflectively versus *CNGA3*- or *CNGB3*-associated achromatopsia with lower cone reflectivity.[133]

In addition to intrinsic variability in reflectivity, photoreceptors also change their reflectance in response to a stimulus.[123,147–151] This property persists over a wide range of modalities, imaging wavelengths, and retinal eccentricities. These stimulus-evoked changes could be used as a metric of photoreceptor health, and efforts to characterize their response properties are ongoing. In particular, it will be important to examine the reflectance response as a function of stimulus properties (e.g., irradiance, duration, wavelength). It has been postulated that changes in a cone's outer segment optical path length are causing the changes in reflectance.[123,142,149] Validated approaches could provide a highly sensitive, noninvasive alternative to electrophysiology to directly monitor photoreceptor structure and/or function.

An inherent challenge in measuring photoreceptor reflectivity is identifying the photoreceptors to be measured. As mentioned above, this often is done using the very reflectivity signal of interest, this intrinsic variability of cones over time as well as the presence of multiple waveguide modes and noncone reflectivity sources (i.e., RPE) severely confound this process. One solution to overcome reduced or ambiguous cone reflectivity is to leverage the reliable cone identification from a corresponding nonconfocal image, and use those coordinates to overlay on a confocal image to identify photoreceptors for subsequent reflectivity measurements. This approach could be attractive especially in areas of cone degeneration, where it can be challenging to identify cones reliably based on their reflectivity alone (e.g., within the transition zone in patients with RP or choroideremia), and further highlights the complementary nature of split-detector and confocal AOSLO.

Investigative Ophthalmology & Visual Science

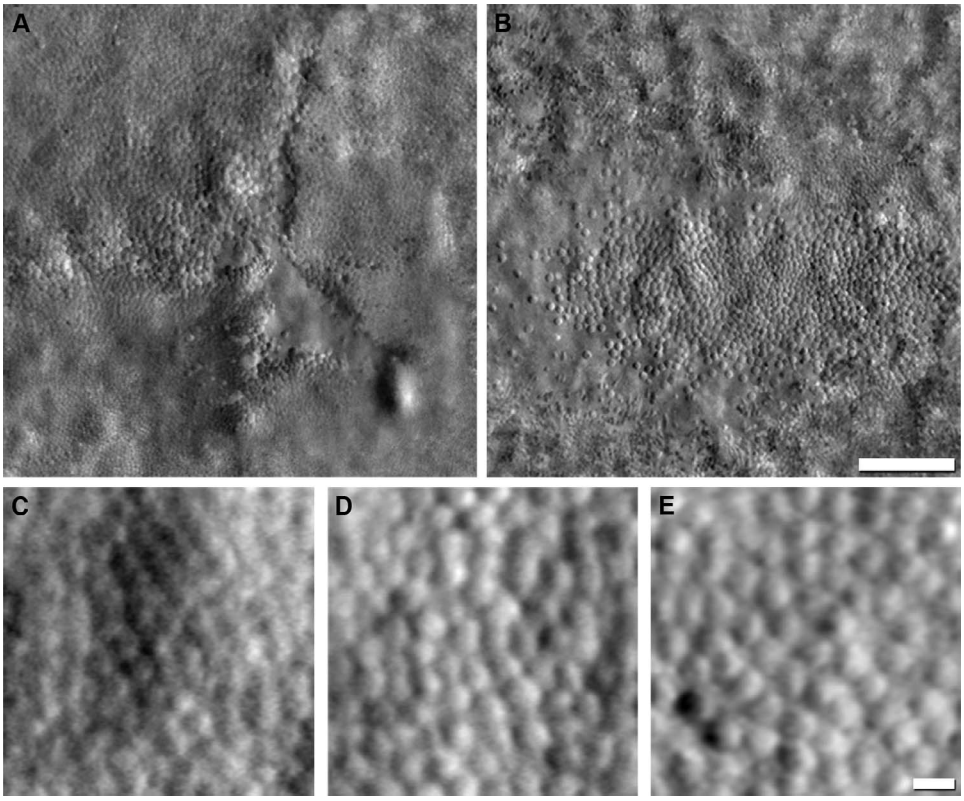

FIGURE 6. Visualizing enlargement of photoreceptor inner segments with split-detector AOSLO. In a normal retina, cones in the fovea typically are not visible using split-detector AOSLO. Foveal images from a subject with closed-globe blunt ocular trauma (**A**) show heterogeneous cone diameters surrounding the central lesion, while images from a subject with *GUCY2D*-associated cone-rod dystrophy (**B**) show a small island of contiguously-packed enlarged cones. Normal cones at 1036 μm (~3°) from the fovea (**C**), compared to enlarged cones within the transition zone from subjects with retinitis pigmentosa (**D**) and choroideremia (**E**) at the same eccentricity as (**C**). *Scale bars*: 100 μm (**A**, **B**) and 10 μm (**C**–**E**). (**A**) and (**B**) are reprinted from Scoles D, Flatter JA, Cooper RF, et al. Assessing photoreceptor structure associated with ellipsoid zone disruptions visualized with optical coherence tomography. *Retina*. 2016;36:91-103. © 2016 by Ophthalmic Communications Society, Inc. (**C**) and (**D**) reprinted from Sun LW, Johnson RD, Langlo CS, et al. Assessing photoreceptor structure in retinitis pigmentosa and Usher syndrome. *Invest Ophthalmol Vis Sci*. 2016;57:2428-2442. Licensed under a Creative Commons Attribution-NonCommercial-NoDerivatives 4.0 International License. (**E**) Reprinted from Sun LW, Johnson RD, Williams V, et al. Multimodal imaging of photoreceptor structure in choroideremia. *PLoS One*. 2016;11:e0167526. Licensed under a Creative Commons Attribution License.

Photoreceptor Size

The process of cone degeneration is fairly well understood in inherited retinal degenerations; histology studies have shown the first structural changes are shortening of the cone outer segments, followed by swelling and degeneration of the inner segment, and finally loss of the cell body.[53,54] Thus, a final photoreceptor-based biomarker to consider is photoreceptor size (e.g., outer segment length and cone diameter). Using OCT, outer segment length has been shown to be abnormal in some diseases, such as albinism[152] and Best disease.[153] Care should be used, as measurement of outer segment length can be affected by light adaptation and segmentation errors of the retinal layers.[154] AO-OCT affords more sensitive measurement of outer segment length than commercial OCT systems, having been used to monitor outer segment renewal on the level of a single cell.[155,156] In addition, it is possible to obtain measurements of cone inner segment diameter using split-detector AOSLO.[51] In our experience, it is difficult to resolve individual cones in the fovea or rods in the normal retina. However, in many pathologic cases in which some cones have been lost, the remaining photoreceptor inner segments enlarge.[53,54,157,158] This often results in easier visualization of foveal cones using split-detector AOSLO imaging (Fig. 6). The enlargement of remnant cones also has been quantified using split-detector AOSLO in patients with choroideremia[20] and RP (Fig. 6).[12] As the ability to assess photoreceptor size is relatively new, it will be interesting to see how it is applied in other retinal degenerations.

Challenges and Looking Forward

The future of clinical trials using AO retinal imaging tools to monitor photoreceptors is promising. To improve the clinical use of AO retinal imaging, the challenges going forward include creating and disseminating automated tools, creating multicenter normative databases, standardizing datasets for comparison, and validating any and all biomarkers, including those that may be developed in the future. In addition, hardware-related issues limit the clinical application of AO retinal imaging. For example, at the time of writing this review, there is no 510k-cleared device, though the rtx1 system from Imagine Eyes (Orsay, France) has received approval in the European Union, Japan, and Australia. While custom laboratory devices are available from Physical Sciences, Inc. (Andover, MA, USA)[159,160] and Boston Micromachines (Boston, MA, USA),[161] the lack of clinical equipment for clinical use in the United States certainly has slowed adoption. Beyond access, there are hardware standardization issues, as the devices available include flood-illuminated AO, AOSLO, and AO-OCT. There has been little work exploring how the different embodiments of

AO retinal imaging relate to each other in the normal and diseased retina, and this limits the ability to conduct multisite studies. Regardless of the modality, the systems should be capable of resolving foveal cones and perifoveal rods to facilitate photoreceptor studies.

Need for Automated Tools

Regardless of the class of biomarker (density/geometry, reflectivity, and size) used, there is a need for automated analytical tools to increase the clinical use of AO retinal imaging. The repeatability and reliability of a photoreceptor-based metric is limited by the ability to detect and identify cones, which often is a required step in quantitative analysis of the photoreceptor mosaic. Manual identification of cones is time-consuming and can result in low repeatability if observers are not experienced in images of retinal disease.[114] For cone identification, many groups have developed methods to detect cones automatically in confocal AOSLO images.[65,69–71,159,162,163] Garrioch et al.[71] showed that manual correction of missed cones from an automated algorithm significantly increased repeatability, though newer automated algorithms have shown comparable repeatability.[68] Automatic cone identification becomes less reliable when rods begin scattering the mosaic or RPE cells become visible in eyes with retinal degeneration. Therefore, automatic photoreceptor algorithms are needed to identify cones and rods within the same image,[68] and to disambiguate multimodal cones from rods in the perifovea. With the distinctive appearance of cones in split-detector AOSLO images, existing algorithms for confocal AOSLO or flood-illuminated AO do not work. An algorithm was developed by Cunefare et al.[67] to identify individual cones in split-detector AOSLO images based on their characteristic pairs of horizontally separated dark and bright regions. The algorithm underestimates high cone density found in healthy eyes, with smaller cones in the fovea, but preliminary performance on irregular mosaics shows promise in characterizing pathology.[67,73] Other algorithms have been published,[164,165] and these efforts represent an important first step in developing robust cone counting software for split-detector images. It again is important to characterize the performance of the specific cone detection algorithm used,[72] as it may affect the subsequent choice of metric for analyzing the mosaic.[87]

Multicenter Normative Databases

For future clinical trials, multicenter normative databases are needed for comparing data sets. Additionally, the AOSLO community lacks photoreceptor mosaic datasets available in the public domain, which would aid in standardization of analyses. Currently, groups have established their own normative data set with their own systems,[107,108,166–168] and few multicenter trials are conducted using identical acquisition systems at all sites. When comparing normative data to eyes with retinal disease, it should be noted that the preferred retinal locus of fixation and peak cone density are not always colocalized in normal[169,170] or in diseased eyes.[103] A static reference point for sampling should be considered if the primary interest of a study is the anatomical fovea, fixation, and/or peak cone density, which may not be located in the same position. In some diseases, one or more foveal landmarks are affected by retinal degeneration and cannot be used; the location of the fovea may be estimated relative to the optic nerve head.[171] Normative databases should include photoreceptor mosaics across various eccentricities aligned to other imaging modalities, along with technical details of each AOSLO system including image scale, field of view, imaging wavelength, and axial length of the subject. This would aid toward cross-site comparisons of analysis algorithms and testing of photoreceptor biomarkers. With comparing data sets comes the challenge of longitudinal alignment of AO retinal images collected over extended time periods, which is an open problem particularly in the actively degenerating retina.

Structure/Function Relationships

For the biomarkers described above to be accepted by the FDA, it will be important to define how they correlate with measures of visual function. However, it is worth keeping in mind that a lack of correlation does not necessarily mean the AO biomarker is not valid, rather in many cases it simply is more sensitive. For example, patients with achromatopsia have no cone function, yet split-detector AOSLO imaging has revealed that remnant cones are present (Fig. 1).[17] One would argue that the structural information only is useful provided it can be extracted with high reliability and repeatability. In addition, cone density is correlated significantly with best-corrected visual acuity and foveal sensitivity, but can decrease by more than a third to a half below normal before visual function becomes abnormal.[11,12] These data suggest that changes in cone spacing/density may be more sensitive biomarkers for assessing therapeutic response. Indeed, Talcott et al.[13] used confocal AOSLO to monitor cone structure after experimental treatment with ciliary neurotrophic factors in patients with RP and demonstrated differences in cone structure between treated and untreated eyes, in the absence of any changes in visual function (e.g., visual acuity, visual field sensitivity, or electroretinographic responses). Future studies should continue to examine how photoreceptor structure (using metrics described in this review) correlates with visual function in a broader range of retinal degenerations.

How can one still have visual function despite the lack of visible cones (e.g., reduced cone density or increased ICD)? There are multiple mechanisms for the visual system to protect vision. The imperfect optics of the eye distort the stimulus; this, along with overlapping receptive fields in the visual system, creates a spatial redundancy in the stimulus.[135] In addition, eyes are moving constantly, including fixational eye movements, to increase visual acuity.[172] Recent studies of eyes with vision loss, including macular telangiectasia,[102] acute idiopathic blind spot enlargement syndrome,[173] and bilateral foveolitis,[140] have demonstrated cones that are not visible using confocal AOSLO imaging, in regions on OCT images with reduced reflectivity or disruption of the ellipsoid zone, but in which the external limiting membrane is visible. If the interface between the outer segments and RPE cells is disrupted, visual function and reflectivity may be reduced, but if the external limiting membrane is visible, cone inner segments (and perhaps abnormally waveguiding outer segments) are present. These "dysflective" cones with abnormal reflective properties on confocal images have reduced, but measurable, visual function,[140] and provide insight into the relationship between the origin of waveguiding cone photoreceptors using confocal AOSLO, OCT, and visual function. These studies highlight the importance of using structural and functional measurements that operate on similar spatial scales—AO microperimetry is an exciting new application that will allow more precise assessment of the relationship between cone structure and function in the living retina.[102,130,140,174–176]

Comparing AO Images to Conventional Clinical Images

In addition to probing the relationship between AO biomarkers and retinal function, examining relationships with routine clinical imaging will be critical to defining the future role of AO

Investigative Ophthalmology & Visual Science

retinal imaging in the clinic. In addition, such comparisons facilitate the interpretation of images across different modalities. For example, a correlation has been observed between hyperautofluorescent changes on fundus autofluorescence imaging and disruption of the IZ on OCT and loss of reflective cone profiles on flood-illuminated AO retinal imaging in RP.[97] Additionally, attenuation of the IZ colocalized with absent cone reflectance on flood-illuminated AO retinal images, and recovery of the IZ accompanied restoration of normal cone reflectance on AO retinal images.[48] In patients with albinism, peak cone density measured with confocal AOSLO has been shown to correlate with foveal outer segment length measured with OCT.[152] Split-detection AOSLO has been shown to identify cones in areas of low or ambiguous ellipsoid zone reflectivity on OCT and confocal AOSLO in a variety of retinal disorders.[16] These studies highlight AO retinal imaging tools as complementary to, rather than a replacement for, conventional clinical imaging modalities.

Conclusions

A multimodal imaging and functional testing approach is necessary for moving forward with clinical trials. AO retinal imaging should have an important role in these efforts, serving as an objective and sensitive method to detect anatomical changes. As the sensitivity of photoreceptor-based metrics exceeds that of conventional tests of visual function, they may be useful in detecting "subclinical" changes over time or in response to treatment. It is important to be mindful of the expected changes to select the photoreceptor-based metric with the appropriate sensitivity. Despite these challenges, we are just at the beginning of the opportunities that AO retinal imaging affords us in understanding retinal diseases on the microscopic scale in vivo, and the ability to monitor photoreceptor density/geometry, reflectivity, and size as outcome measures in clinical trials. The future is bright for using sensitive metrics to monitor photoreceptors well before vision changes in inherited retinal diseases.

Acknowledgments

The authors thank Margaret Strampe and Brian Higgins for their assistance.

Supported by the National Center for Advancing Translational Sciences and the National Eye Institute of the National Institutes of Health (NIH; Bethesda, MD, USA) under award numbers UL1TR001436, R01EY024969, R01EY017607, P30EY001931, and P30EY002162, and by Foundation Fighting Blindness and Research to Prevent Blindness (Nelson Trust Award for Retinitis Pigmentosa to JLD and an Unrestricted Grant to UCSF). The authors alone are responsible for the content and writing of this paper.

Disclosure: **K.M. Litts**, None; **R.F. Cooper**, None; **J.L. Duncan**, Neurotech USA, Inc. (F), AGTC (C), Spark Therapeutics (C), jCyte (C), Novelion (C), Ionis (C), SparingVision (C); **J. Carroll**, AGTC (F), MeiraGTx (C), OptoVue (F)

References

1. Csaky KG, Richman EA, Ferris FL III. Report from the NEI/FDA ophthalmic clinical trial design and endpoints symposium. *Invest Ophthalmol Vis Sci*. 2008;49:479–489.
2. Berson EL. Long-term visual prognoses in patients with retinitis pigmentosa: the Ludwig von Sallmann lecture. *Exp Eye Res*. 2007;85:7–14.
3. Fishman GA, Jacobson SG, Alexander KR, et al. Outcome measures and their application in clinical trials for retinal degenerative diseases: outline, review, and perspective. *Retina*. 2005;25:772–777.
4. Grover S, Fishman GA, Anderson RJ, Alexander KR, Derlacki DJ. Rate of visual field loss in retinitis pigmentosa. *Ophthalmology*. 1997;104:460–465.
5. Marcos S, Werner JS, Burns SA, et al. Vision science and adaptive optics, the state of the field. *Vision Res*. 2017;132:3–33.
6. Roorda A, Duncan JL. Adaptive optics ophthalmoscopy. *Ann Rev Vis Sci*. 2015;1:19–50.
7. Liang J, Williams DR, Miller D. Supernormal vision and high-resolution retinal imaging through adaptive optics. *J Opt Soc Am A Opt Image Sci Vis*. 1997;14:2884–2892.
8. Jonnal RS, Kocaoglu OP, Zawadzki RJ, Liu Z, Miller DT, Werner JS. A review of adaptive optics optical coherence tomography: technical advances, scientific applications, and the future. *Invest Ophthalmol Vis Sci*. 2016;57:OCT51–OCT68.
9. Felberer F, Kroisamer JS, Baumann B, et al. Adaptive optics SLO/OCT for 3D imaging of human photoreceptors in vivo. *Biomed Opt Express*. 2014;5:439–456.
10. Stepien KE, Han DP, Schell J, Godara P, Rha J, Carroll J. Spectral-domain optical coherence tomography and adaptive optics may detect hydroxychloroquine retinal toxicity before symptomatic vision loss. *Trans Am Ophthalmol Soc*. 2009;107:28–34.
11. Ratnam K, Carroll J, Porco TC, Duncan JL, Roorda A. Relationship between foveal cone structure and clinical measures of visual function in patients with inherited retinal degenerations. *Invest Ophthalmol Vis Sci*. 2013;54:5836–5847.
12. Sun LW, Johnson RD, Langlo CS, et al. Assessing photoreceptor structure in retinitis pigmentosa and Usher syndrome. *Invest Ophthalmol Vis Sci*. 2016;57:2428–2442.
13. Talcott KE, Ratnam K, Sundquist S, et al. Longitudinal study of cone photoreceptors during retinal degeneration and in response to ciliary neurotrophic factor treatment. *Invest Ophthalmol Vis Sci*. 2011;52:2219–2226.
14. Stepien KE, Martinez WM, Dubis AM, Cooper RF, Dubra A, Carroll J. Subclinical photoreceptor disruption in response to severe head trauma. *Arch Ophthalmol*. 2012;130:400–402.
15. Flatter JA, Cooper RF, Dubow MJ, et al. Outer retinal structure after closed-globe blunt ocular trauma. *Retina*. 2014;34:2133–2146.
16. Scoles D, Flatter JA, Cooper RF, et al. Assessing photoreceptor structure associated with ellipsoid zone disruptions visualized with optical coherence tomography. *Retina*. 2016;36:91–103.
17. Langlo CS, Patterson EJ, Higgins BP, et al. Residual foveal cone structure in *CNGB3*-associated achromatopsia. *Invest Ophthalmol Vis Sci*. 2016;57:3984–3995.
18. Syed R, Sundquist SM, Ratnam K, et al. High-resolution images of retinal structure in patients with choroideremia. *Invest Ophthalmol Vis Sci*. 2013;54:950–961.
19. Langlo CS, Erker LR, Parker M, et al. Repeatability and longitudinal assessment of foveal cone structure in *CNGB3*-associated achromatopsia [published online ahead of print January 31, 2017]. *Retina*. doi:10.1097/IAE.0000000000001434.
20. Sun LW, Johnson RD, Williams V, et al. Multimodal imaging of photoreceptor structure in choroideremia. *PLoS One*. 2016;11:e0167526.
21. Morgan JI, Han G, Klinman E, et al. High-resolution adaptive optics retinal imaging of cellular structure in choroideremia. *Invest Ophthalmol Vis Sci*. 2014;55:6381–6397.
22. Sincich LC, Zhang Y, Tiruveedhula P, Horton JC, Roorda A. Resolving single cone inputs to visual receptive fields. *Nat Neurosci*. 2009;12:967–969.

23. Geng Y, Dubra A, Yin L, et al. Adaptive optics retinal imaging in the living mouse eye. *Biomed Opt Express*. 2012;3:715–734.
24. Guevara-Torres A, Williams DR, Schallek JB. Imaging translucent cell bodies in the living mouse retina without contrast agents. *Biomed Opt Express*. 2015;6:2106–2119.
25. Huckenpahler AL, Wilk MA, Cooper RF, et al. Imaging the adult zebrafish cone mosaic using optical coherence tomography. *Vis Neurosci*. 2016;33:E011.
26. Pennesi ME, Garg AK, Feng S, et al. Measuring cone density in a Japanese macaque (*Macaca fuscata*) model of age-related macular degeneration with commercially available adaptive optics. *Adv Exp Med Biol*. 2014;801:309–316.
27. Sharma R, Schwarz C, Williams DR, Palczewska G, Palczewski K, Hunter JJ. In vivo two-photon fluorescence kinetics of primate rods and cones. *Invest Ophthalmol Vis Sci*. 2016;57:647–657.
28. Sajdak B, Sulai YN, Langlo CS, et al. Noninvasive imaging of the thirteen-lined ground squirrel photoreceptor mosaic. *Vis Neurosci*. 2016;33:e003.
29. Jacobson SG, Aleman TS, Cideciyan AV, et al. Identifying photoreceptors in blind eyes caused by *RPE65* mutations: prerequisite for human gene therapy success. *Proc Natl Acad Sci U S A*. 2005;102:6177–6182.
30. Morgan JIW, Dubra A, Wolfe R, Merigan WH, Williams DR. In vivo autofluorescence imaging of the human and macaque retinal pigment epithelial cell mosaic. *Invest Ophthalmol Vis Sci*. 2009;50:1350–1359.
31. Scoles D, Sulai YN, Dubra A. In vivo dark-field imaging of the retinal pigment epithelium cell mosaic. *Biomed Opt Express*. 2013;4:1710–1723.
32. Liu Z, Kocaoglu OP, Miller DT. 3D imaging of retinal pigment epithelial cells in the living human retina. *Invest Ophthalmol Vis Sci*. 2016;57:OCT533–OCT543.
33. Bedggood P, Metha A. Analysis of contrast and motion signals generated by human blood constituents in capillary flow. *Opt Lett*. 2014;39:610–613.
34. Chui TY, Vannasdale DA, Burns SA. The use of forward scatter to improve retinal vascular imaging with an adaptive optics scanning laser ophthalmoscope. *Biomed Opt Express*. 2012;3:2537–2549.
35. Rossi EA, Granger CE, Sharma R, et al. Imaging individual neurons in the retinal ganglion cell layer of the living eye. *Proc Natl Acad Sci U S A*. 2017;114:586–591.
36. Morgan JIW. The fundus photo has met its match: optical coherence tomography and adaptive optics ophthalmoscopy are here to stay. *Ophthalmic Physiol Opt*. 2016;36:218–239.
37. Pinhas A, Dubow M, Shah N, et al. In vivo imaging of human retinal microvasculature using adaptive optics scanning light ophthalmoscope fluorescein angiography. *Biomed Opt Express*. 2013;4:1305–1317.
38. Spaide RF. Questioning optical coherence tomography. *Ophthalmology*. 2012;119:2203–2204.
39. Jonnal RS, Kocaoglu OP, Zawadzki RJ, Lee SH, Werner JS, Miller DT. The cellular origins of the outer retinal bands in optical coherence tomography images. *Invest Ophthalmol Vis Sci*. 2014;55:7904–7918.
40. Meadway A, Girkin CA, Zhang Y. A dual-modal retinal imaging system with adaptive optics. *Opt Express*. 2013;21:29792–29807.
41. Roorda A, Williams DR. Optical fiber properties of individual human cones. *J Vis*. 2002;2:404–412.
42. Enoch J, Tobey FL. *Vertebrate Photoreceptor Optics*. Berlin: Springer-Verlag; 1981.
43. Pallikaris A, Williams DR, Hofer H. The reflectance of single cones in the living human eye. *Invest Ophthalmol Vis Sci*. 2003;44:4580–4592.
44. Liu Z, Kocaoglu OP, Turner TL, Miller DT. Modal content of living human cone photoreceptors. *Biomed Opt Express*. 2015;6:3378–3404.
45. Marcos S, Burns SA. Cone spacing and waveguide properties from cone directionality measurements. *J Opt Soc Am A Opt Image Sci Vis*. 1999;16:995–1004.
46. Vohnsen B. Directional sensitivity of the retina: a layered scattering model of outer-segment photoreceptor pigments. *Biomed Opt Express*. 2014;5:1569–1587.
47. Rativa D, Vohnsen B. Simulating human photoreceptor optics using a liquid-filled photonic crystal fiber. *Biomed Opt Express*. 2011;2:543–551.
48. Jacob J, Paques M, Krivosic V, et al. Meaning of visualizing retinal cone mosaic on adaptive optics images. *Am J Ophthalmol*. 2015;159:118–123.e1.
49. Staurenghi G, Sadda S, Chakravarthy U, Spaide RF, Panel IO. Proposed lexicon for anatomic landmarks in normal posterior segment spectral-domain optical coherence tomography: The IN•OCT consensus. *Ophthalmology*. 2014;121:1572–1578.
50. Roorda A, Zhang Y, Duncan JL. High-resolution in vivo imaging of the RPE mosaic in eyes with retinal disease. *Invest Ophthalmol Vis Sci*. 2007;48:2297–2303.
51. Scoles D, Sulai YN, Langlo CS, et al. In vivo imaging of human cone photoreceptor inner segments. *Invest Ophthalmol Vis Sci*. 2014;55:4244–4251.
52. Elsner A, Miura M, Burns S, et al. Multiply scattered light tomography and confocal imaging: detecting neovascularization in age-related macular degeneration. *Opt Express*. 2000;7:95–106.
53. Milam AH, Li ZY, Fariss RN. Histopathology of the human retina in retinitis pigmentosa. *Prog Retin Eye Res*. 1998;17:175–205.
54. Ross JW, Fernandez de Castro JP, Zhao J, et al. Generation of an inbred miniature pig model of retinitis pigmentosa. *Invest Ophthalmol Vis Sci*. 2012;53:501–507.
55. Syed N, Smith JE, John SK, Seabra MC, Aguirre GD, Milam AH. Evaluation of retinal photoreceptors and pigment epithelium in a female carrier of choroideremia. *Ophthalmology*. 2001;108:711–720.
56. Flannery JG, Bird AC, Farber DB, Weleber RG, Bok D. A histopathologic study of a choroideremia carrier. *Invest Ophthalmol Vis Sci*. 1990;31:229–236.
57. Johnson PT, Lewis GP, Talaga KC, et al. Drusen-associated degeneration in the retina. *Invest Ophthalmol Vis Sci*. 2003;44:4481–4488.
58. Litts KM, Wang X, Clark ME, et al. Exploring photoreceptor reflectivity through multimodal imaging of outer retinal tubulation in advanced age-related macular degeneration. *Retina*. 2017;37:978–988.
59. Curcio CA, Sloan KR. Packing geometry of human cone photoreceptors: variation with eccentricity and evidence for local anisotropy. *Vis Neurosci*. 1992;9:169–180.
60. Pum D, Ahnelt PK, Grasl M. Iso-orientation areas in the foveal cone mosaic. *Vis Neurosci*. 1990;5:511–523.
61. Sawides L, de Castro A, Burns SA. The organization of the cone photoreceptor mosaic measured in the living human retina. *Vision Res*. 2017;132:34–44.
62. Cooper RF, Lombardo M, Carroll J, Sloan KR, Lombardo G. Methods for investigating the local spatial anisotropy and the preferred orientation of cones in adaptive optics retinal images. *Vis Neurosci*. 2016;33:E005.
63. Yellott JI Jr. Spectral analysis of spatial sampling by photoreceptors: Topological disorder prevents aliasing. *Vision Res*. 1982;22:1205–1210.
64. Coletta NJ, Williams DR. Psychophysical estimate of extrafoveal cone spacing. *J Opt Soc Am A*. 1987;4:1503–1513.

Investigative Ophthalmology & Visual Science

65. Cooper RF, Langlo CS, Dubra A, Carroll J. Automatic detection of modal spacing (Yellott's ring) in adaptive optics scanning light ophthalmoscope images. *Ophthalmic Physiol Opt*. 2013;33:540–549.
66. Williams DR, Coletta NJ. Cone spacing and the visual resolution limit. *J Opt Soc Am A*. 1987;4:1514–1523.
67. Cunefare D, Cooper RF, Higgins B, et al. Automatic detection of cone photoreceptors in split detector adaptive optics scanning light ophthalmoscope images. *Biomed Opt Express*. 2016;7:2036–2050.
68. Chiu SJ, Lokhnygina Y, Dubis AM, et al. Automatic cone photoreceptor segmentation using graph theory and dynamic programming. *Biomed Opt Express*. 2013;4:924–937.
69. Xue B, Choi SS, Doble N, Werner JS. Photoreceptor counting and montaging of en-face retinal images from an adaptive optics fundus camera. *J Opt Soc Am A Opt Image Sci Vis*. 2007;24:1364–1372.
70. Li KY, Roorda A. Automated identification of cone photoreceptors in adaptive optics retinal images. *J Opt Soc Am A Opt Image Sci Vis*. 2007;24:1358–1363.
71. Garrioch R, Langlo C, Dubis AM, Cooper RF, Dubra A, Carroll J. Repeatability of in vivo parafoveal cone density and spacing measurements. *Optom Vis Sci*. 2012;89:632–643.
72. Mariotti L, Devaney N. Performance analysis of cone detection algorithms. *J Opt Soc Am A Opt Image Sci Vis*. 2015;32:497–506.
73. Cunefare D, Fang L, Cooper RF, Dubra A, Carroll J, Farsiu S. Open source software for automatic detection of cone photoreceptors in adaptive optics ophthalmoscopy using convolutional neural networks. *Sci Rep*. 2017;7:6620.
74. Li KY, Tiruveedhula P, Roorda A. Intersubject variability of foveal cone photoreceptor density in relation to eye length. *Invest Ophthalmol Vis Sci*. 2010;51:6858–6867.
75. Song H, Chui TY, Zhong Z, Elsner AE, Burns SA. Variation of cone photoreceptor packing density with retinal eccentricity and age. *Invest Ophthalmol Vis Sci*. 2011;52:7376–7384.
76. Chui TYP, Song HX, Burns SA. Individual variations in human cone photoreceptor packing density: variations with refractive error. *Invest Ophthalmol Vis Sci*. 2008;49:4679–4687.
77. Dees EW, Dubra A, Baraas RC. Variability in parafoveal cone mosaic in normal trichromatic individuals. *Biomed Opt Express*. 2011;2:1351–1358.
78. Lombardo M, Lombardo G, Schiano Lomoriello D, Ducoli P, Stirpe M, Serrao S. Interocular symmetry of parafoveal photoreceptor cone density. *Retina*. 2013;33:1640–1649.
79. Hansen SO, Cooper RF, Dubra A, Carroll J, Weinberg DV. Selective cone photoreceptor injury in acute macular neuroretinopathy. *Retina*. 2013;33:1650–1658.
80. Park SP, Chung JK, Greenstein V, Tsang SH, Chang S. A study of factors affecting the human cone photoreceptor density measured by adaptive optics scanning laser ophthalmoscope. *Exp Eye Res*. 2013;108:1–9.
81. Menghini M, Lujan BJ, Zayit-Soudry S, et al. Correlation of outer nuclear layer thickness with cone density values in patients with retinitis pigmentosa and healthy subjects. *Invest Ophthalmol Vis Sci*. 2014;56:372–381.
82. Duncan JL, Zhang Y, Gandhi J, et al. High-resolution imaging with adaptive optics in patients with inherited retinal degeneration. *Invest Ophthalmol Vis Sci*. 2007;48:3283–3291.
83. Roorda A, Metha AB, Lennie P, Williams DR. Packing arrangement of the three cone classes in primate retina. *Vision Res*. 2001;41:1291–1306.
84. Roorda A, Romero-Borja F, Donnelly WJ III, Queener H, Hebert T, Campbell M. Adaptive optics scanning laser ophthalmoscopy. *Opt Express*. 2002;10:405–412.
85. Yoon MK, Roorda A, Zhang Y, et al. Adaptive optics scanning laser ophthalmoscopy images in a family with the mitochondrial DNA T8993C mutation. *Invest Ophthalmol Vis Sci*. 2009;50:1838–1847.
86. Mkrtchyan M, Lujan BJ, Merino D, Thirkill CE, Roorda A, Duncan JL. Outer retinal structure in patients with acute zonal occult outer retinopathy. *Am J Ophthalmol*. 2012;153:757–768.
87. Cooper RF, Wilk MA, Tarima S, Carroll J. Evaluating descriptive metrics of the human cone mosaic. *Invest Ophthalmol Vis Sci*. 2016;57:2992–3001.
88. Lombardo M, Parravano M, Serrao S, Ziccardi L, Giannini D, Lombardo G. Investigation of adaptive optics imaging biomarkers for detecting pathological changes of the cone mosaic in patients with type 1 diabetes mellitus. *PLoS One*. 2016;11:e0151380.
89. Zayit-Soudry S, Duncan JL, Syed R, Menghini M, Roorda AJ. Cone structure imaged with adaptive optics scanning laser ophthalmoscopy in eyes with nonneovascular age-related macular degeneration. *Invest Ophthalmol Vis Sci*. 2013;54:7498–7509.
90. Land ME, Cooper RF, Young J, et al. Cone structure in subjects with known genetic relative risk for AMD. *Optom Vis Sci*. 2014;91:939–949.
91. Ratnam K, Västinsalo H, Roorda A, Sankila E-MK, Duncan JL. Cone structure in patients with Usher syndrome type III and mutations in the *Clarin 1* gene. *JAMA Ophthalmol*. 2013;131:67–74.
92. Jacob J, Krivosic V, Paques M, Tadayoni R, Gaudric A. Cone density loss on adaptive optics in early macular telangiectasia type 2. *Retina*. 2016;36:545–551.
93. Razeen MM, Cooper RF, Langlo CS, et al. Correlating photoreceptor mosaic structure to clinical findings in Stargardt disease. *Trans Vis Sci Tech*. 2016;5(2):6.
94. Chen YF, Roorda A, Duncan JL. Advances in imaging of Stargardt disease. *Adv Exp Med Biol*. 2010;664:333–340.
95. Pang CE, Suqin Y, Sherman J, Freund KB. New insights into Stargardt disease with multimodal imaging. *Ophthalmic Surg Lasers Imaging Retina*. 2015;46:257–261.
96. Baraas RC, Carroll J, Gunther KL, et al. Adaptive optics retinal imaging reveals S-cone dystrophy in tritan color-vision deficiency. *J Opt Soc Am A Opt Image Sci Vis*. 2007;24:1438–1447.
97. Gale MJ, Feng S, Titus HE, Smith TB, Pennesi ME. Interpretation of flood-illuminated adaptive optics images in subjects with retinitis pigmentosa. *Adv Exp Med Biol*. 2016;854:291–297.
98. Ziccardi L, Giannini D, Lombardo G, et al. Multimodal approach to monitoring and investigating cone structure and function in an inherited macular dystrophy. *Am J Ophthalmol*. 2015;160:301–312.e6.
99. Choi SS, Doble N, Hardy JL, et al. In vivo imaging of the photoreceptor mosaic in retinal dystrophies and correlations with visual function. *Invest Ophthalmol Vis Sci*. 2006;47:2080–2092.
100. Ueno S, Nakanishi A, Kominami T, et al. In vivo imaging of a cone mosaic in a patient with achromatopsia associated with a *GNAT2* variant. *Jpn J Ophthalmol* 2017;61:92–98.
101. Langlo CS, Flatter JA, Dubra A, Wirostko WJ, Carroll J. A lensing effect of inner retinal cysts on images of the photoreceptor mosaic. *Retina*. 2014;34:421–422.
102. Wang Q, Tuten WS, Lujan BJ, et al. Adaptive optics microperimetry and OCT images show preserved function and recovery of cone visibility in macular telangiectasia type 2 retinal lesions. *Invest Ophthalmol Vis Sci*. 2015;56:778–786.
103. Duncan JL, Ratnam K, Birch DG, et al. Abnormal cone structure in foveal schisis cavities in X-linked retinoschisis from mutations in exon 6 of the *RS1* gene. *Invest Ophthalmol Vis Sci*. 2011;52:9614–9623.

Investigative Ophthalmology & Visual Science

104. Hasegawa T, Ooto S, Makiyama Y, Hata M, Miyamoto K, Yoshimura N. Circinate partition-like findings on cone mosaic imaged by adaptive optics scanning laser ophthalmoscopy in eyes with inner nuclear layer microcystic changes [published online ahead of print March 13, 2017]. *Retin Cases Brief Rep*. doi:10.1097/ICB.0000000000000564.
105. Lombardo M, Serrao S, Ducoli P, Lombardo G. Eccentricity dependent changes of density, spacing and packing arrangement of parafoveal cones. *Ophthalmic Physiol Opt*. 2013;33:516–526.
106. Dubra A, Sulai Y, Norris JL, et al. Noninvasive imaging of the human rod photoreceptor mosaic using a confocal adaptive optics scanning ophthalmoscope. *Biomed Opt Express*. 2011;2:1864–1876.
107. Wells-Gray EM, Choi SS, Bries A, Doble N. Variation in rod and cone density from the fovea to the mid-periphery in healthy human retinas using adaptive optics scanning laser ophthalmoscopy. *Eye (Lond)*. 2016;30:1135–1143.
108. Merino D, Duncan JL, Tiruveedhula P, Roorda A. Observation of cone and rod photoreceptors in normal subjects and patients using a new generation adaptive optics scanning laser ophthalmoscope. *Biomed Opt Express*. 2011;2:2189–2201.
109. Bidaut Garnier M, Flores M, Debellemanière G, et al. Reliability of cone counts using an adaptive optics retinal camera. *Clin Exp Ophthalmol*. 2014;42:833–840.
110. Zayit-Soudry S, Sippl-Swezey N, Porco T, et al. Repeatability of cone spacing measures in eye with inherited retinal degenerations. *Invest Ophthalmol Vis Sci*. 2015;56:6179–6189.
111. Lombardo M, Parravano M, Lombardo G, et al. Adaptive optics imaging of parafoveal cones in type 1 diabetes. *Retina*. 2014;34:546–557.
112. Tanna P, Kasilian M, Strauss R, et al. Reliability and repeatability of cone density measurements in patients with Stargardt disease and RPGR-associated retinopathy. *Invest Ophthalmol Vis Sci*. 2017;58:3608–3615.
113. Liu BS, Tarima S, Visotcky A, et al. The reliability of parafoveal cone density measurements. *Br J Ophthalmol*. 2014;98:1126–1131.
114. Abozaid MA, Langlo CS, Dubis AM, Michaelides M, Tarima S, Carroll J. Reliability and repeatability of cone density measurements in patients with congenital achromatopsia. *Adv Exp Med Biol*. 2016;854:277–283.
115. Cooper RF, Sulai YN, Dubis AM, et al. Effects of intraframe distortion on measures of cone mosaic geometry from adaptive optics scanning light ophthalmoscopy. *Trans Vis Sci Tech*. 2016;5(1):10.
116. Wade AR, Fitzke FW. In vivo imaging of the human cone-photoreceptor mosaic using a confocal laser scanning ophthalmoscope. *Lasers Light Ophthalmol*. 1998;8:129–136.
117. Vogel CR, Arathorn DW, Roorda A, Parker A. Retinal motion estimation in adaptive optics scanning laser ophthalmoscopy. *Opt Express*. 2006;14:487–497.
118. Huang G, Zhong Z, Zou W, Burns SA. Lucky averaging: quality improvement of adaptive optics scanning laser ophthalmoscope images. *Opt Lett*. 2011;36:3786–3788.
119. Salmon AE, Cooper RF, Langlo CS, Baghaie A, Dubra A, Carroll J. An automated reference frame selection (ARFS) algorithm for cone imaging with adaptive optics scanning light ophthalmoscopy. *Trans Vis Sci Tech*. 2017;6(2):9.
120. Sheehy CK, Yang Q, Arathorn DW, Tiruveedhula P, de Boer JF, Roorda A. High-speed, image-based eye tracking with a scanning laser ophthalmoscope. *Biomed Opt Express*. 2012;3:2611–2622.
121. Sheehy CK, Tiruveedhula P, Sabesan R, Roorda A. Active eye-tracking for an adaptive optics scanning laser ophthalmoscope. *Biomed Opt Express*. 2015;6:2412–2423.
122. Lu J, Gu B, Wang X, Zhang Y. High-speed adaptive optics line scan confocal retinal imaging for human eye. *PLoS One*. 2017;12:e0169358.
123. Rha J, Jonnal RS, Thorn KE, Qu J, Zhang Y, Miller DT. Adaptive optics flood-illumination camera for high speed retinal imaging. *Opt Express*. 2006;14:4552–4569.
124. Feng S, Gale MJ, Fay JD, et al. Assessment of different sampling methods for measuring and representing macular cone density using flood-illuminated adaptive optics. *Invest Ophthalmol Vis Sci*. 2015;56:5751–5763.
125. Lombardo M, Serrao S, Ducoli P, Lombardo G. Influence of sampling window size and orientation on parafoveal cone packing density. *Biomed Opt Express*. 2013;4:1318–1331.
126. Lombardo M, Serrao S, Lombardo G. Technical factors influencing cone packing density estimates in adaptive optics flood illuminated retinal images. *PLoS One*. 2014;9:e107402.
127. Curcio CA, Sloan KR, Kalina RE, Hendrickson AE. Human photoreceptor topography. *J Comp Neurol*. 1990;292:497–523.
128. Larocca F, Nankivil D, Farsiu S, Izatt JA. Handheld simultaneous scanning laser ophthalmoscopy and optical coherence tomography system. *Biomed Opt Express*. 2013;4:2307–2321.
129. Godara P, Cooper RF, Sergouniotis PI, et al. Assessing retinal structure in complete congenital stationary night blindness and Oguchi disease. *Am J Ophthalmol*. 2012;154:987–1001.
130. Bruce KS, Harmening WM, Langston BR, Tuten WS, Roorda A, Sincich LC. Normal perceptual sensitivity arising from weakly reflective cone photoreceptors. *Invest Ophthalmol Vis Sci*. 2015;56:4431–4438.
131. Song H, Rossi EA, Latchney L, et al. Cone and rod loss in Stargardt disease revealed by adaptive optics scanning light ophthalmoscopy. *JAMA Ophthalmol*. 2015;133:1198–1203.
132. Carroll J, Choi SS, Williams DR. In vivo imaging of the photoreceptor mosaic of a rod monochromat. *Vision Res*. 2008;48:2564–2568.
133. Dubis AM, Cooper RF, Aboshiha J, et al. Genotype-dependent variability in residual cone structure in achromatopsia: Towards developing metrics for assessing cone health. *Invest Ophthalmol Vis Sci*. 2014;55:7303–7311.
134. Genead MA, Fishman GA, Rha J, et al. Photoreceptor structure and function in patients with congenital achromatopsia. *Invest Ophthalmol Vis Sci*. 2011;52:7298–7308.
135. Makous W, Carroll J, Wolfing JI, Lin J, Christie N, Williams DR. Retinal microscotomas revealed with adaptive-optics microflashes. *Invest Ophthalmol Vis Sci*. 2006;47:4160–4167.
136. Mariotti L, Devaney N, Lombardo G, Lombardo M. Understanding the changes of cone reflectance in adaptive optics flood illumination retinal images over three years. *Biomed Opt Express*. 2016;7:2807–2822.
137. Rativa D, Vohnson B. Analysis of individual cone-photoreceptor directionality using scanning laser ophthalmoscopy. *Biomed Opt Express*. 2011;2:1423–1431.
138. Zweifel SA, Engelbert M, Laud K, Margolis R, Spaide RF, Freund KB. Outer retinal tubulation: a novel optical coherence tomography finding. *Arch Ophthalmol*. 2009;127:1596–1602.
139. Panorgias A, Zawadzki RJ, Capps AG, Hunter AA, Morse LS, Werner JS. Multimodal assessment of microscopic morphology and retinal function in patients with geographic atrophy. *Invest Ophthalmol Vis Sci*. 2013;54:4372–4384.
140. Tu JH, Foote KG, Lujan BJ, et al. Dysflective cones: visual function and cone reflectivity in long-term follow-up of acute bilateral foveolitis. *Am J Ophthalmol Case Rep*. 2017;7:14–19.

Investigative Ophthalmology & Visual Science

141. Pircher M, Kroisamer JS, Felberer F, Sattmann H, Götzinger E, Hitzenberger CK. Temporal changes of human cone photoreceptors observed in vivo with SLO/OCT. *Biomed Opt Express*. 2010;2:100–112.
142. Jonnal RS, Besecker JR, Derby JC, et al. Imaging outer segment renewal in living human cone photoreceptors. *Opt Express*. 2010;18:5257–5270.
143. Jonnal RS, Rha J, Zhang Y, Cense B, Gao W, Miller DT. Functional imaging of single cone photoreceptors using an adaptive optics flood illumination camera. *Invest Ophthalmol Vis Sci*. 2007;48:1955.
144. Cooper RF, Dubis AM, Pavaskar A, Rha J, Dubra A, Carroll J. Spatial and temporal variation of rod photoreceptor reflectance in the human retina. *Biomed Opt Express*. 2011;2:2577–2589.
145. Sabesan R, Hofer H, Roorda A. Characterizing the human cone photoreceptor mosaic via dynamic photopigment densitometry. *PLoS One*. 2015;10:e0144891.
146. Hirota M, Miyagawa S, Kanda H, et al. Slow cone reflectance changes during bleaching determined by adaptive optics scanning laser ophthalmoscope in living human eyes. *PLoS One*. 2015;10:e0131485.
147. Rha J, Schroeder B, Godara P, Carroll J. Variable optical activation of human cone photoreceptors visualized using short coherence light source. *Opt Lett*. 2009;34:3782–3784.
148. Li Y-G, Zhang Q-X, Liu L, Amthor FR, Yao X-C. High spatiotemporal resolution imaging of fast intrinsic optical signals activated by retinal flicker stimulation. *Opt Express*. 2010;18:7210–7218.
149. Jonnal RS, Rha J, Zhang Y, Cense B, Gao W, Miller DT. In vivo functional imaging of human cone photoreceptors. *Opt Express*. 2007;14:16141–16160.
150. Hillmann D, Spahr H, Pfaffle C, Sudkamp H, Franke G, Huttmann G. In vivo optical imaging of physiological responses to photostimulation in human photoreceptors. *Proc Natl Acad Sci U S A*. 2016;113:13138–13143.
151. Grieve K, Roorda A. Intrinsic signals from human cone photoreceptors. *Invest Ophthalmol Vis Sci*. 2008;49:713–719.
152. Wilk MA, Wilk BM, Langlo CS, Cooper RF, Carroll J. Evaluating outer segment length as a surrogate measure of peak foveal cone density. *Vision Res*. 2017;130:57–66.
153. Abràmoff MD, Mullins RF, Lee K, et al. Human photoreceptor outer segments shorten during light adaptation. *Invest Ophthalmol Vis Sci*. 2013;54:3721–3728.
154. Stepien KE, Kay DB, Carroll J. Outer segment length in different best disease genotypes–reply. *JAMA Ophthalmol* 2014;132:1153.
155. Kocaoglu OP, Lee S, Jonnal RS, et al. Imaging cone photoreceptors in three dimensions and in time using ultrahigh resolution optical coherence tomography with adaptive optics. *Biomed Opt Express*. 2011;2:748–763.
156. Jonnal R, Kocaoglu OP, Wang Q, Lee S, Miller DT. Phase-sensitive imaging of the outer retina using optical coherence tomography and adaptive optics. *Biomed Opt Express*. 2012; 3:104–124.
157. Curcio CA, Medeiros NE, Millican CL. Photoreceptor loss in age-related macular degeneration. *Invest Ophthalmol Vis Sci*. 1996;37:1236–1249.
158. Litts KM, Messinger JD, Freund KB, Zhang Y, Curcio CA. Inner segment remodeling and mitochondrial translocation in cone photoreceptors in age-related macular degeneration with outer retinal tubulation. *Invest Ophthalmol Vis Sci*. 2015;56:2243–2253.
159. Mujat M, Ferguson RD, Iftimia N, Hammer DX. Compact adaptive optics line scanning ophthalmoscope. *Opt Express*. 2009;17:10242–10258.
160. Hammer DX, Ferguson RD, Mujat M, Iftimia NV, inventors; Physical Sciences, Inc., assignee. Adaptive optics line scanning ophthalmoscope. US patent 8201943-B2. June 19, 2012.
161. Nesper PL, Scarinci F, Fawzi AA. Adaptive optics reveals photoreceptor abnormalities in diabetic macular ischemia. *PLoS One*. 2017;12:e0169926.
162. Lazareva A, Liatsis P, Rauscher FG. Hessian-LoG filtering for enhancement and detection of photoreceptor cells in adaptive optics retinal images. *J Opt Soc Am A Opt Image Sci Vis*. 2016;33:84–94.
163. Bukowska DM, Chew AL, Huynh E, et al. Semi-automated identification of cones in the human retina using circle Hough transform. *Biomed Opt Express*. 2015;6:4676–4693.
164. Liu J, Dubra A, Tam J. A fully automatic framework for cell segmentation on non-confocal adaptive optics images. *Proceedings of SPIE*; 2016;9785:97852J.
165. Bergeles C, Dubis AM, Davidson B, et al. Unsupervised identification of cone photoreceptors in non-confocal adaptive optics scanning light ophthalmoscope images. *Biomed Opt Express*. 2017;8:3081.
166. Elsner AE, Chui TY, Feng L, Song HX, Papay JA, Burns SA. Distribution differences of macular cones measured by AOSLO: Variation in slope from fovea to periphery more pronounced than differences in total cones. *Vision Res*. 2017;132:62–68.
167. Zhang T, Godara P, Blancob ER, et al. Variability in human cone topography assessed by adaptive optics scanning laser ophthalmoscopy. *Am J Ophthalmol*. 2015;160:290–300.
168. Wilk MA, McAllister JT, Cooper RF, et al. Relationship between foveal cone specialization and pit morphology in albinism. *Invest Ophthalmol Vis Sci*. 2014;55:4186–4198.
169. Wilk MA, Dubis AM, Cooper RF, Summerfelt P, Dubra A, Carroll J. Assessing the spatial relationship between fixation and foveal specializations. *Vision Res*. 2017;132:53–61.
170. Putnam NM, Hofer HJ, Doble N, Chen L, Carroll J, Williams DR. The locus of fixation and the foveal cone mosaic. *J Vis*. 2005;5:632–639.
171. Rohrschneider K. Determination of the location of the fovea on the fundus. *Invest Ophthalmol Vis Sci*. 2004;45:3257–3258.
172. Ratnam K, Domdei N, Harmening WM, Roorda A. Benefits of retinal image motion at the limits of spatial vision. *J Vis*. 2017;17(1):30.
173. Horton JC, Parker AB, Botelho JV, Duncan JL. Spontaneous regeneration of human photoreceptor outer segments. *Sci Rep*. 2015;5:12364.
174. Tuten WS, Tiruveedhula P, Roorda A. Adaptive optics scanning laser ophthalmoscope-based microperimetry. *Optom Vis Sci*. 2012;89:563–574.
175. Harmening WM, Tuten WS, Roorda A, Sincich LC. Mapping the perceptual grain of the human retina. *J Neurosci*. 2014; 34:5667–5677.
176. Sabesan R, Schmidt BP, Tuten WS, Roorda A. The elementary representation of spatial and color vision in the human retina. *Sci Adv*. 2016;2:e1600797.

Investigative Ophthalmology & Visual Science